processes

MDPI

Article

Adsorption and Reaction Mechanisms of Direct Palladium Synthesis by ALD Using $Pd(hfac)_2$ and Ozone on Si (100) Surface

Chunyu Cheng, Yiming Zou, Jiahui Li, Amanda Jiamin Ong, Ronn Goei, Jingfeng Huang, Shuzhou Li * and Alfred Iing Yoong Tok *

School of Materials Science and Engineering, Nanyang Technological University, Singapore 639798, Singapore; chunyu.cheng@ntu.edu.sg (C.C.); yiming004@ntu.edu.sg (Y.Z.); jiahui.li@ntu.edu.sg (J.L.); jiamin.ong@ntu.edu.sg (A.J.O.); ronn_goei@ntu.edu.sg (R.G.); huang_jingfeng@rp.edu.sg (J.H.)
* Correspondence: lisz@ntu.edu.sg (S.L.); miytok@ntu.edu.sg (A.I.Y.T.)

Abstract: Palladium nanoparticles made by atomic layer deposition (ALD) normally involve formaldehyde or H_2 as a reducing agent. Since formaldehyde is toxic and H_2 is explosive, it is advantageous to remove this reducing step during the fabrication of palladium metal by ALD. In this work we have successfully used $Pd(hfac)_2$ and ozone directly to prepare palladium nanoparticles, without the use of reducing or annealing agents. Density functional theory (DFT) was employed to explore the reaction mechanisms of palladium metal formation in this process. DFT results show that $Pd(hfac)_2$ dissociatively chemisorbed to form Pd(hfac)* and hfac* on the Si (100) surface. Subsequently, an O atom of the ozone could cleave the C–C bond of Pd(hfac)* to form Pd* with a low activation barrier of 0.46 eV. An O atom of the ozone could also be inserted into the hfac* to form Pd(hfac-O)* with a lower activation barrier of 0.29 eV. With more ozone, the C–C bond of Pd(hfac-O)* could be broken to produce Pd* with an activation barrier of 0.42 eV. The ozone could also chemisorb on the Pd atom of Pd(hfac-O)* to form O_3-Pd(hfac-O)*, which could separate into O-Pd(hfac-O)* with a high activation barrier of 0.83 eV. Besides, the activation barrier was 0.64 eV for Pd* that was directly oxidized to PdOx by ozone. Based on activation barriers from DFT calculations, it was possible to prepare palladium without reducing steps when ALD conditions were carefully controlled, especially the ozone parameters, as shown by our experimental results. The mechanisms of this approach could be used to prepare other noble metals by ALD without reducing/annealing agents.

Keywords: DFT study; palladium; ozone; atomic layer deposition

Citation: Cheng, C.; Zou, Y.; Li, J.; Ong, A.J.; Goei, R.; Huang, J.; Li, S.; Tok, A.I.Y. Adsorption and Reaction Mechanisms of Direct Palladium Synthesis by ALD Using $Pd(hfac)_2$ and Ozone on Si (100) Surface. *Processes* **2021**, *9*, 2246. https://doi.org/10.3390/pr9122246

Academic Editor: Gianvito Vilé

Received: 4 November 2021
Accepted: 26 November 2021
Published: 13 December 2021

1. Introduction

Atomic layer deposition (ALD) is widely used in many fields, owing to the fact that the large and complex 3D film surfaces can be used to grow nanoparticles uniformally and conformally over them. This can be done with precise control of the film thickness and nanoparticle size [1–3], where the films and nanoparticles chemisorb on the substrate surface with a strong binding. Many noble metals at the nanoscale have been synthesized successfully by ALD [4–8]. Among them, palladium has a wide range of applications at the nanoscale for catalysts [9,10], hydrogen storage [11–13], and sensors [14–16]. It is desirable in most of the applications to prepare uniform and conformal palladium particles on complex surfaces to improve palladium content per unit volume [17–19]. Elam et al. [20] have reported a method to nucleate and grow palladium directly on the surface of Al_2O_3 using $Pd(hfac)_2$ (hfac = hexafluoroacetylacetone) and formalin (the aqueous solution of formaldehyde) by ALD. Weber et al. [21] have prepared palladium particles with high purity and low resistivity at 100~200 °C using $Pd(hfac)_2$ and H_2 plasma followed by an O_2 plasma step, where the O_2 plasma step was necessary to remove hydrocarbon fragments on the surface that remained after the H_2 plasma step. Since formaldehyde is

toxic, and hydrogen gas is explosive, as well as plasma ALD equipment being expensive, an alternative method to prepare palladium particles by ALD is desirable.

Ozone has been used as a co-reactant to prepare noble metals by ALD. Dendooven et al. [22] grew thin platinum films using ALD at 100–300 °C by (methylcyclopentadienyl)trimethylplatinum and ozone. They found that the platinum film was uniform with low impurity levels and close-to-bulk resistivity. Hämäläinen et al. [23] reported that thin amorphous platinum oxide films were deposited at 120 and 130 °C using ALD by platinum(II) bis(acetylacetonate) and ozone, while metallic platinum films were obtained at 140 °C and above. By changing the oxygen flow, Park et al. [24] controlled the formation of Ru and RuO_2 using ALD by bis (cyclopentadienyl) ruthenium and oxygen. Therefore, ozone might be a good candidate to prepare palladium particles with $Pd(hfac)_2$ without reducing steps. In our previous work [25], palladium metal was prepared using $Pd(hfac)_2$ and ozone by ALD. However, the reaction mechanisms between $Pd(hfac)_2$ and ozone on the surface of the substrate were still not clear.

In this work, calculations based on density functional theory (DFT) were carried out to investigate the precursor adsorption and reaction mechanisms of direct palladium synthesis by $Pd(hfac)_2$ and ozone on an Si (100) surface; palladium was synthesized successfully on the Si (100) surface. $Pd(hfac)_2$ precursors first chemisorb on the Si (100) surface, which is accompanied by its dissociation to form Pd(hfac)* and hfac*. Pd* could be obtained through a low activation barrier of 0.46 eV by an O atom of the ozone by breaking the C–C bond of Pd(hfac)*. Pd(hfac-O)* could also be produced through a lower activation barrier of 0.29 eV, where an O atom of the ozone was substituted for the O atom of the Pd–O–C bonds in Pd(hfac)*. Pd(hfac-O)* could further react with an ozone molecule to form Pd* with an activation barrier of 0.42 eV, where an O atom of the ozone could cleave the C–C bond of Pd(hfac-O)*. An ozone molecule could also be directly absorbed on Pd(hfac)*, which could also occur to form O_3-Pd(hfac-O)*, which was reversible and barrierless. The dissociation of O_3-Pd(hfac-O)* into O-Pd(hfac-O)* and O_2 had a high activation barrier of 0.83 eV, where O-Pd(hfac-O)* could lead to PdO_x eventually. Another possible pathway to form PdO_x was the oxidation of the fabricated Pd* by ozone, which also had a high activation barrier of 0.64 eV. Therefore, the preparation of Pd metal through ALD could be realized by $Pd(hfac)_2$ and ozone with controlled conditions, which was also confirmed by our experiment.

2. Procedures

2.1. Model

First-principal DFT calculations were used. The Vienna Ab Initio Simulation Package [26,27] (VASP) was used to execute the projector augmented wave (PAW) method [28,29] and generalized gradient approximation (GGA) [30]. Up to 400eV of energy cutoff was employed for the plane-wave basis set. The absolute value of force on each unconstrained atom <0.001 eV/Å was carried out for geometry optimization. The Brillouin zone was sampled using a Monkhorst-Pack 2 × 2 × 1 k-point mesh [31]. The nudged elastic band (NEB) method was used to obtain the transition-state structure to simulate the minimum-energy profile along the reaction pathway connecting the reactant and product [32,33].

A simpler dissociation process for the adsorbed $Pd(hfac)_2$ (referred to as "$Pd(hfac)_2$*") (Reaction (1)) was considered in this work [34]. The reaction energy ΔE_{re1} for the reaction is shown in Equation (2). The adsorption energy $\Delta E_{ads\text{-}species}$ of $Pd(hfac)_2$, Pd(hfac), or hfac on the Si (100) surface was calculated as shown in Equation (3).

$$Pd(hfac)_2* + * \rightarrow Pd(hfac) * + hfac* \quad (1)$$

where $Pd(hfac)*$ and $hfac*$ represent the adsorbed Pd(hfac) and hfac. The asterisk symbol means open surface, as defined below for $E_{surface}$.

$$\Delta E_{re1} = E_{Pd(hfac)*} + E_{hfac*} - E_{surface} - E_{Pd(hfac)_2*} \quad (2)$$

where $E_{Pd(hfac)*}$, E_{hfac*}, and $E_{Pd(hfac)_2*}$ were the total energies of Pd(hfac)*, hfac*, and Pd(hfac)$_2$* respectively.

$$\Delta E_{ads\text{-}species} = E_{species*} - E_{surface} - E_{species(g)} \quad (3)$$

where $E_{species*}$ was the total energy of Pd(hfac)$_2$*, Pd(hfac)*, or hfac*. $E_{species}$ represented the chemical potential of the Pd(hfac)$_2$, Pd(hfac), or hfac.

Consistent with other studies [35,36] simulating the actual substrate, a reconstructed Si (100) slab that consisted of seven layers, with a vacuum space of 15 Å, was used. The bottom three Si layers were kept fixed at their bulk positions to represent the infinitely large solid, while the other atomic layers were relaxed. Seven different adsorption sites were considered on the clean Si (100) surface as shown in Figure 1a—top 1 (T1), top 2 (T2), bridge 1 (B1), bridge 2 (B2), bridge 3 (B3), hollow 1 (H1), and hollow 2 (H2). Different adsorption orientations of species were then carried out for each of the sites. The height of the species was set at h_0 = 3 Å for all structures, as shown in Figure 1b.

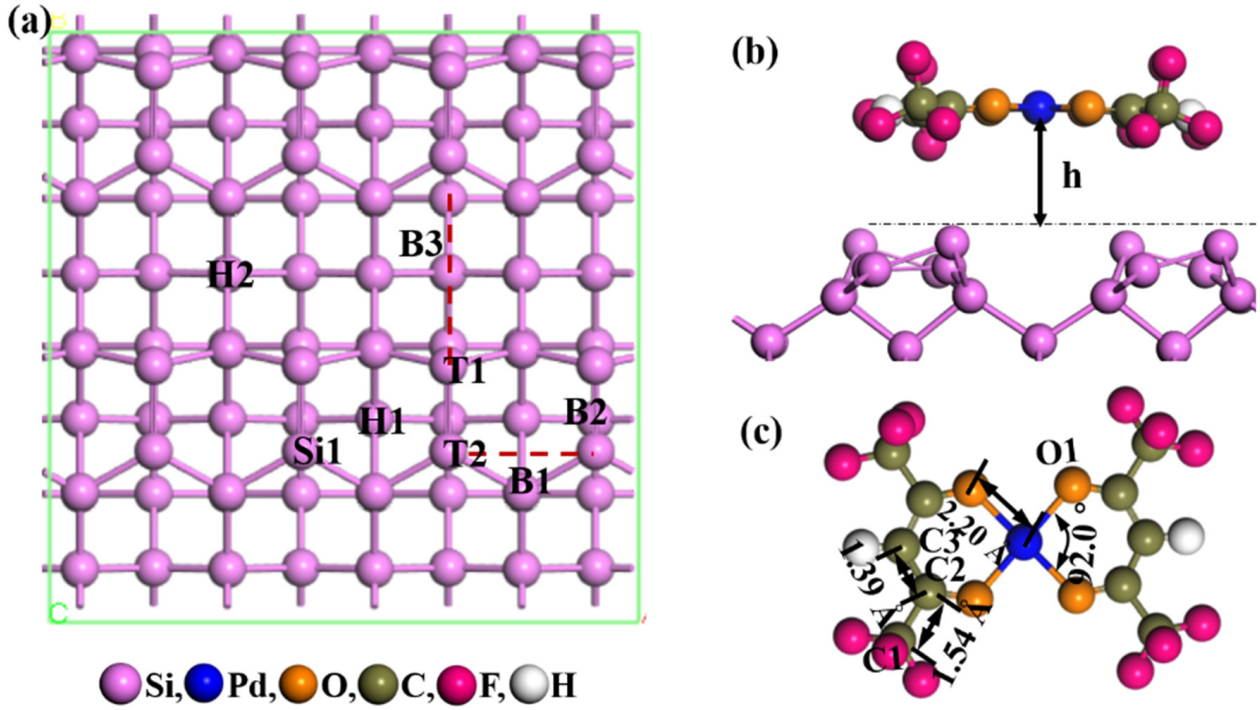

Figure 1. (**a**) The surface of the obtained clean Si (100) after geometry optimization, (**b**) the structure of clean Si (100) with a Pd(hfac)$_2$ (h_0 = 3.0 Å), and (**c**) the obtained Pd(hfac)$_2$ after geometry optimization.

2.2. Experiment

Si (100) substrates (10 mm × 10 mm × 0.2 mm) were washed sequentially under ultrasonication in ethanol, acetone, and iso-propyl alcohol (IPA), then dried with nitrogen flow. Subsequently, Si (100) substrates were placed in the ALD reactor. Nitrogen (99.999%) was used as a carrier and as a purging gas. The ALD deposition was carried out in a low-pressure ALD reactor under a nitrogen pressure of about 1 mbar. Pd(hfac)$_2$ (Strem Chemicals) and ozone gas were added sequentially into the ALD reactor heated at 200 °C. The precursor was heated to 60 °C. The transfer line connecting the bubbler to the ALD reactor was heated to 100 °C to avoid condensation of the precursor gas. The ALD cycle consisted of two 0.4 s pulses of Pd(hfac)$_2$ and a 5 s purge, followed by one 0.2 s pulse of ozone and a 5 s purge. A total of 1000 cycles were used to prepare the palladium particles. Ozone with the concentration of 0.87 g m^{-3} was used, lower than that in our previous work [25].

The crystalline structure of the particles was estimated using grazing incidence X-ray diffraction (GIXRD). The data were collected with a MAR345 2D imaging detector using a 12.7 KeV X-ray source with an incident angle of 1°. We also measured the GIXRD pattern of the substrates by the same way in order to subtract the diffraction from the substrates around the coated areas. The elemental composition and chemical bonding structure of the resulted particles were measured by X-ray photoelectron spectroscopy (XPS, Axis supra) using an Al Kα source. Ar ion sputtering was carried out to remove the topmost impurities. The morphology of the particles was analyzed by scanning electron microscopy (SEM, JEOL JSM-7600F).

3. Results and Discussion

3.1. Chemical Adsorption of Pd(hfac)$_2$ on the Clean Si (100) Surface

In a typical ALD process, the precursors are first chemisorbed on the reactive sites, resulting in the release of by-products. Figure 1c shows the optimized structure of Pd(hfac)$_2$. Pd coordinated four oxygens of two hfac ligands. The length of the covalent Pd-O bonds was 2.00 Å and the mean angle of O-Pd-O was 92.0°. Bond lengths for C1–C2 and C2–C3 were 1.54 and 1.39 Å respectively, these are shown in Figure 1c. The results were consistent with experimental and DFT results that have been reported [37,38].

DFT calculation was used to explain the adsorption and reaction mechanisms of Pd(hfac)$_2$ on the clean Si (100) surface. Mulliken bond populations with 3.0 Å distance cut-offs were then carried out to assess the relative strength of the bonds; higher positive bond population value implied a stronger bond strength. The B2 site had the most stable configuration for the adsorption of Pd(hfac)$_2$ on the Si (100) surface, with an adsorption energy of −2.79 eV, as shown in Figure 2a. The Pd(hfac)$_2$* was significantly distorted from planarity to improve the adsorption stability and was associated with the dissociative adsorption of Pd(hfac)$_2$. Pd atom then bonded with two neighboring Si atoms to annihilate the dangling bonds. The lengths of the Pd–Si bonds were 2.22~2.28 Å, and the populations were estimated to be 0.20~0.23, which implied strong bonds. The Pd–O bonds had been weakened, as bond lengths increased to 2.23~2.45 Å.

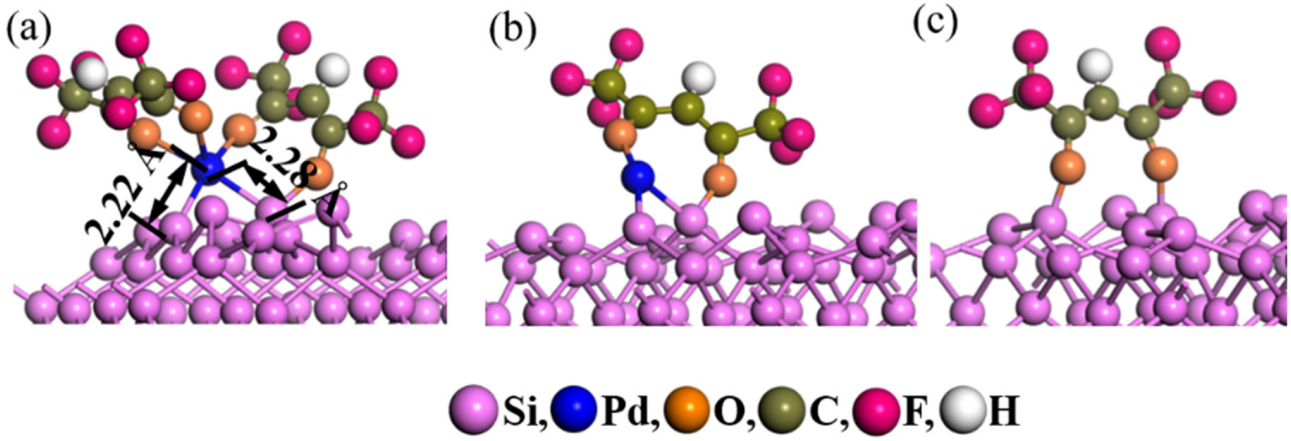

Figure 2. The obtained clean Si (100) with (**a**) Pd(hfac)$_2$*, (**b**) Pd(hfac)* or (**c**) hfac* after geometry optimization.

The reaction energy for Reaction (1) was −1.87 eV. DFT calculations performed showed that Pd(hfac)$_2$* dissociated to Pd(hfac)* and hfac*. The optimized structures are shown in Figure 2b,c. The lowest adsorption energy of Pd(hfac) on the clean Si (100) surface was −4.08 eV. After Pd(hfac) was adsorped at the B2 site, two Pd–Si bonds were formed. The coordination configuration of Pd was preserved with a coordination number of 3. Figure 2c shows the most stable structure of hfac adsorption on the Si. Hfac preferentially adsorbed with the perpendicular species axis at the B1 site with an adsorption energy of −4.21 eV. The two carbonyl groups of hfac* adsorbed on two neighboring Si atoms.

3.2. Surface Reaction between Pd(hfac) and Ozone

Ligands are expected to remain intact upon adsorption so they can subsequently volatilize the metal atoms to be removed by the co-reactant. The reaction between Pd(hfac)* and ozone was studied since $Pd(hfac)_2$* dissociated to produce Pd(hfac)* and hfac*. Figures 3 and 4 show the potential energy profiles and optimized reactant, transition state, and product structures. There were two reaction pathways as the ozone approached (step 1, Figure 3). One activation barrier of the reaction between the ozone and Pd(hfac)* was 0.46 eV (green lines). The relaxed adsorption structure with adsorption energy −3.01 eV is shown in Figure 4. The O atom of the ozone adsorbed above the bridging C2–C3 site (as marked in Figure 1c) to form an epoxide (the inset in Figure 4) and then underwent a dissociative chemisorption process. The O–C3 bond and oxygen molecule were formed on the surface (the transition state 1 inset in Figure 4). This was consistent with DFT calculations and infrared spectroscopy of the reaction between trimethylaluminum and ozone [39,40] The distance between the O1 (as marked in Figure 1c) and Pd atoms of Pd(hfac)* increased from 2.12 Å to 4.09 Å as the C2–C3 bond was broken. This indicated that the O1–Pd bond was cleaved. As a result, the formed complex dissociated into the adsorbed Pd, CF_3–OC, and CF_3–CO–CHO (referred to as "Pd*", "CF_3–OC*", and "CF_3–CO–CHO*", respectively). Gaseous fragments of the ligand could be formed. C atoms (except for the C atom of $–CF_3$) might have been oxidized into CO_2 and H atoms might have been oxidized to form H_2O [21].

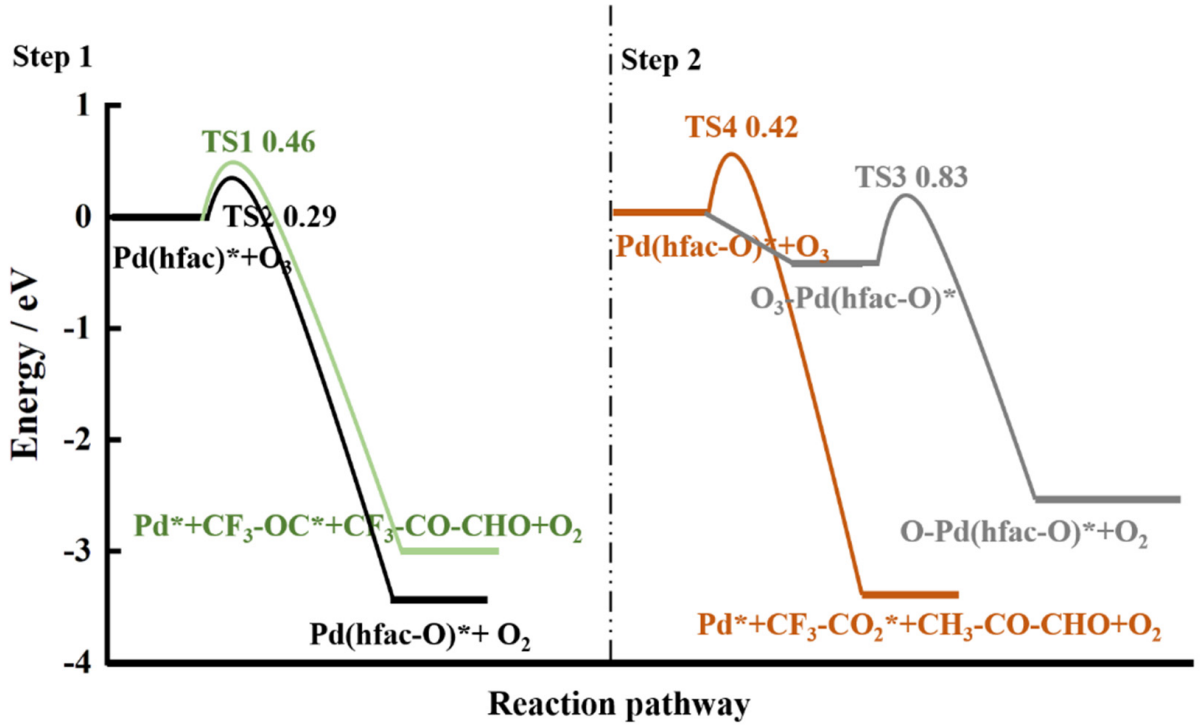

Figure 3. Energy profile of the reaction of ozone with (**a**) Pd(hfac)* (step 1) or (**b**) Pd(hfac-O)* (step 2) on clean Si (100) surface.

The other reaction between the ozone and Pd(hfac)* at the toping Pd site hadw a 0.29 eV activation barrier, thus was kinetically favorable (black lines). The O in the ozone was reactive towards the Pd in Pd(hfac)*. The distance between the O1 and the Pd atom then increased from 2.12 Å to 4.50 Å, suggesting that the O1–Pd bond was split. The O1–Si bond was formed from the transfer of the residual electrons on the O to the topmost Si atom. The adsorbed O of the ozone bonds with the C2 atom also caused the chemically adsorbed Pd(hfac-O) (referred to as "Pd(hfac-O)*") and oxygen formation, through an adsorption energy of −3.46 eV.

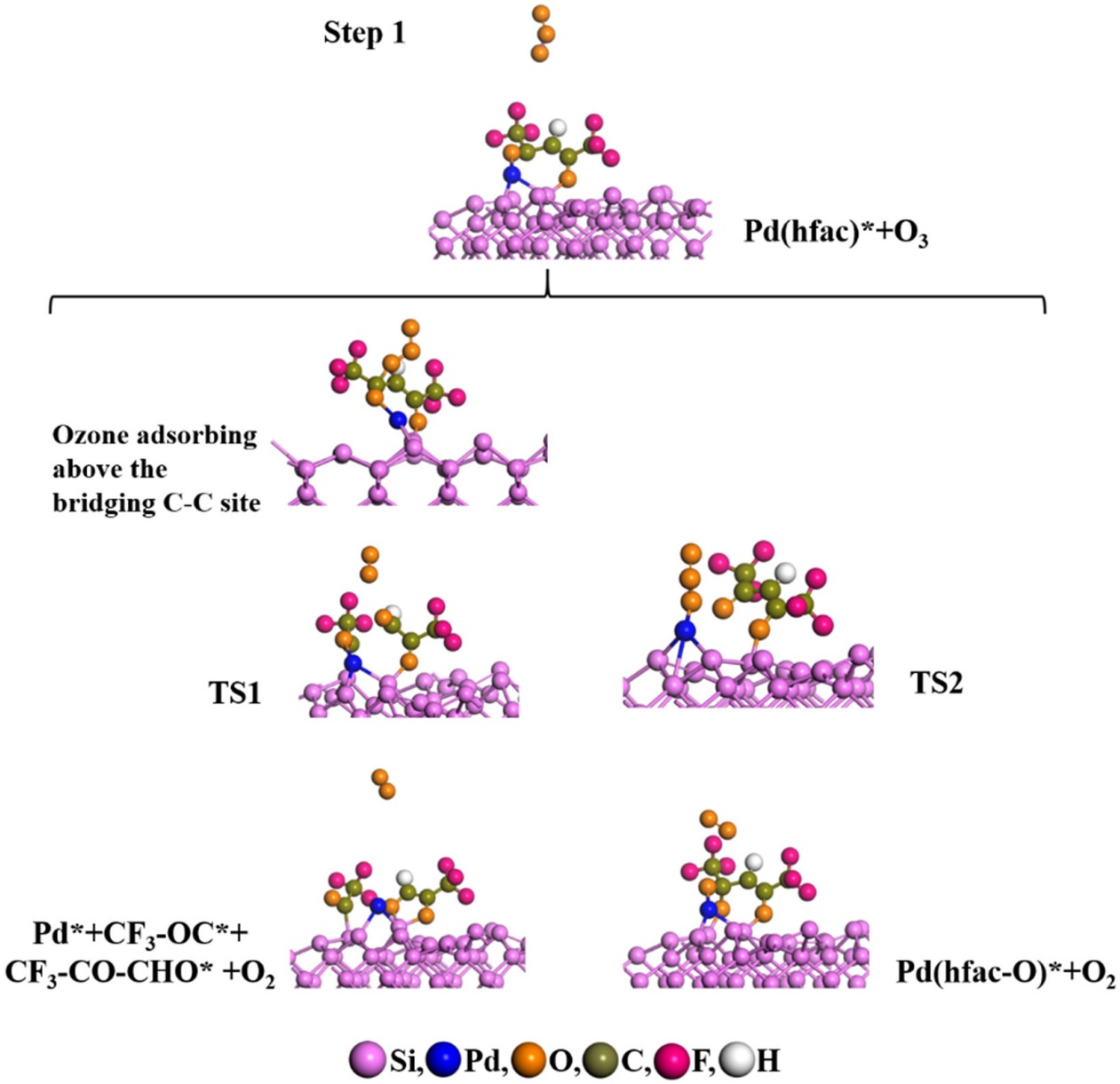

Figure 4. Reaction between Pd(hfac)* and ozone on the clean Si (100) surface represented by snapshots.

There were two reaction pathways as another ozone approached the Pd(hfac-O)*, (step 2, Figure 3). Figure 5 shows the optimized reactant, transition state, and product structures. The reaction between ozone and Pd(hfac)-O* at the C–C bridging position could have formed a stable structure with an activation barrier of 0.42 eV and adsorption energy of −3.14 eV, shown in Figure 3 (orange lines) and Figure 5, which was similar to the reaction described in Figure 3 (green lines) and Figure 4. The final products were Pd*, adsorbed CF_3–CO_2, and CF_3–CO–CHO*. The latter two might then have been oxidized to form CO_2, H_2O, and gaseous fluoride.

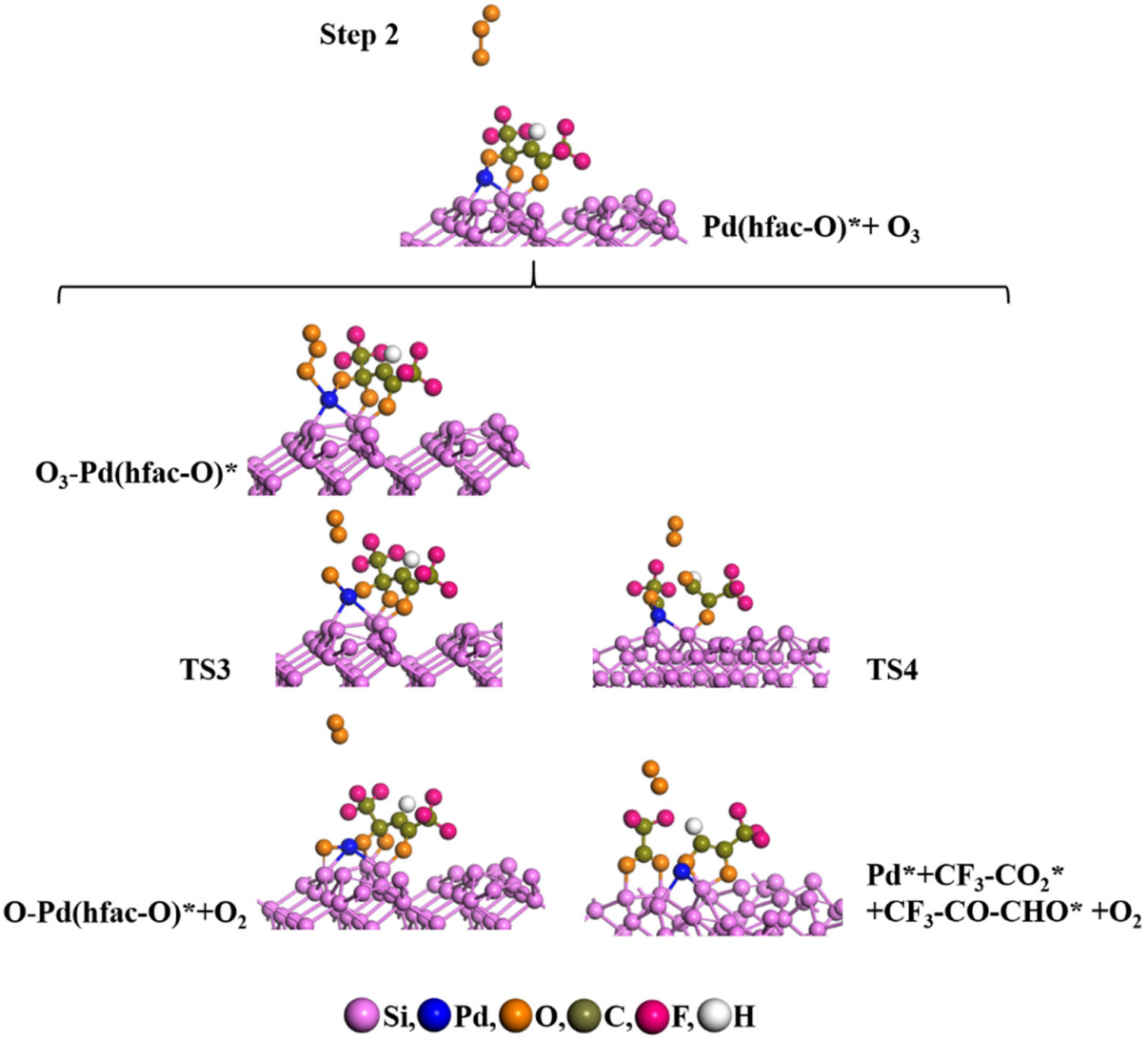

Figure 5. Reaction between Pd(hfac-O)* and ozone on the clean Si (100) surface represented by snapshots.

O_3–Pd(hfac-O)* formation could also have resulted as the O in the ozone was adsorbed barrierless at the toping Pd position, with adsorption energy of −0.58 eV, shown in Figure 5. Since ozone prefers to be broken down into an oxygen molecule after the atomic O adsorption, the decomposition of O_3–Pd(hfac-O)* was assumed (reaction (4)). The reaction energy for Reaction (4) could be written as: $\Delta E_{re4} = E_{O\text{–}Pd(hfac-O)*} + E_{O_2} - E_{O_3\text{–}Pd(hfac-O)*}$. The obtained reaction energy was −2.06 eV, implying that further decomposition was favorable. The activation barrier of the decomposition reaction was 0.83 eV (gray lines), almost twice as high as that of the reaction between ozone and Pd(hfac-O)* displayed in Figure 3 (orange lines). Thus, it was more difficult to produce PdO than Pd, resulting in less PdO in the Pd metal, which was consistent with the previous report [25]. The relaxed adsorption structure is shown in Figure 5 (O–Pd(hfac)* + O_2). An O atom of ozone adsorbed at the toping Pd site and then an oxygen molecule was produced (the transition state 3 inset in Figure 5), which underwent a dissociative chemisorption process. The distance between the adsorbed O and Pd atoms decreased from 2.14 Å to 2.00 Å as the oxygen molecule formed. Besides, since Si was a tetravalent species and the Si atom bonding with the Pd atom had one dangling bond left, the Si atom bonds with the adsorbed an O atom to improve its structural stability. Hence, the formed complex dissociated into the adsorbed O–Pd(hfac) (referred to as "O–Pd(hfac)*") and an oxygen molecule.

$$O_3\text{–}Pd(hfac-O)* \rightarrow O\text{–}Pd(hfac-O)* + O_2 \quad (4)$$

Atomic Pd moves might have occurred as the ligand was consumed. The most stable structure of atomic Pd adsorption on the Si surface is shown in Figure 6. Pd atom preferred to adsorb at the H1 site with an adsorption energy of −0.21 eV, as it was the most efficient annihilation of the dangling bonds.

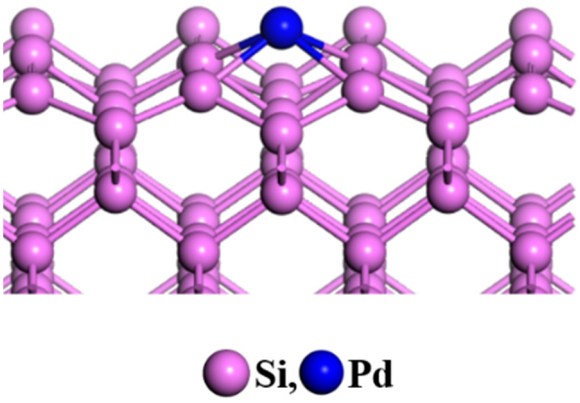

Figure 6. The obtained clean Si (100) with a Pd atom after geometry optimization.

Excess ozone might have reacted with Pd* directly with an activation barrier of 0.64 eV (Figure 7), lower than the activation barrier of the decomposition of O_3–Pd(hfac-O)* (gray lines in Figure 3). Thus, the reaction between Pd* and the ozone was also an important reason for the generation of PdO. Figure 7 shows the optimized reactant, transition state, and product structures. The O atom of the ozone, located at the bridging Pd–Si site, preferentially bonded with the Pd and Si atoms to terminate two surface-dangling bonds, causing the formation of Pd–O–Si. Meanwhile, the distance between the O_2 and O_3 atoms (marked in Figure 7) increased from 1.28 Å to 2.55 Å, indicating that the O_2–O_3 bond was broken and an oxygen molecule was formed. The final adsorption energy was −2.64 eV. Hence, excess ozone caused the formation of PdO.

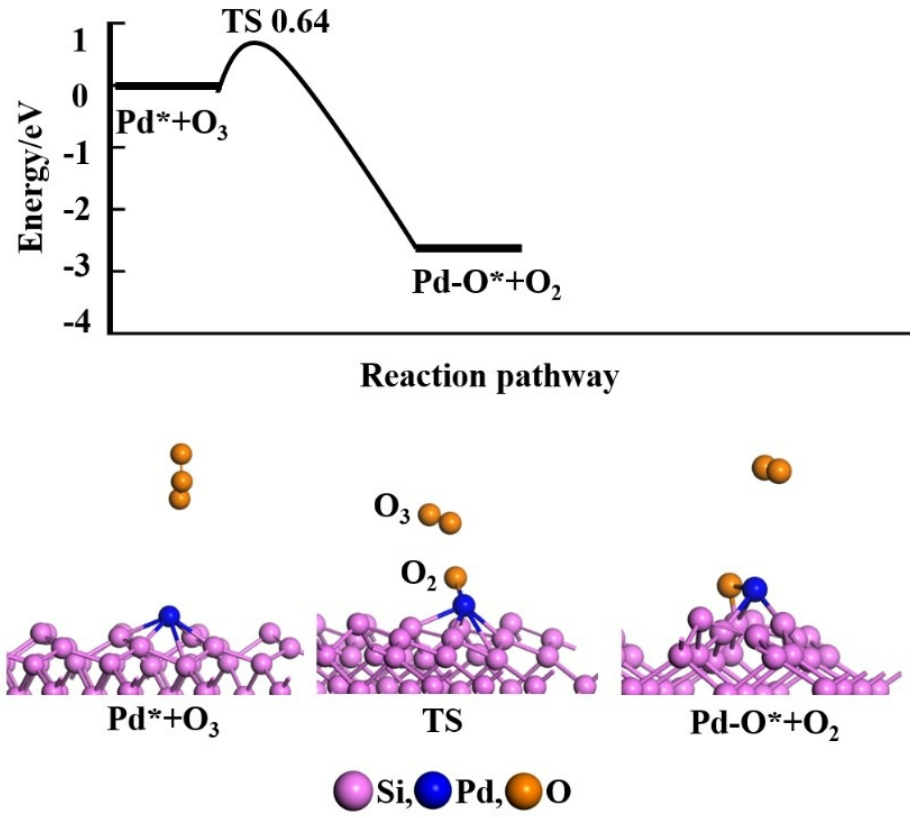

Figure 7. Energy profile of the reaction of ozone with Pd* on clean Si (100) surface.

In conclusion, palladium metal can be synthesized when the ozone concentration is carefully controlled. Palladium metal should be prepared with less ozone.

3.3. Experiment Results

The adsorption and dissociation of $Pd(hfac)_2$ on the hydroxylated Si (100) surface was similar to those on clean Si (100) surfaces. This is because the OH* group is not the adsorption site of $Pd(hfac)_2$ according to a study on the effect of substrates' surface conditions on adsorption and reaction mechanisms of $Pd(hfac)_2$ on Si (100) surfaces, as described in the Supporting Information. Hence, palladium metal can be prepared on the Si (100) surface without specific surface treatment (e.g., heat treatment or H_2SO_4/H_2O_2 mixture) by ALD. Thus, Si (100) substrates cleaned by ethanol, acetone, and IPA were used. Figure 8a presents a typical SEM surface image of the particles prepared on the Si (100) surface. The particles' diameters were 10~20 nm, indicating that palladium nucleated as discrete islands and grew laterally with increased ALD cycles. The GIXRD pattern (bottom-left corner in Figure 8a) shows that the particles had the face-centered cubic (fcc) crystal structure. Meanwhile, Pd (111), Pd (200), Pd (202), and Pd (311) planes were observed, which was consistent with the literature's report [21]. Hence, palladium was grown on the Si (100) surface, which was consistent with the simulation results.

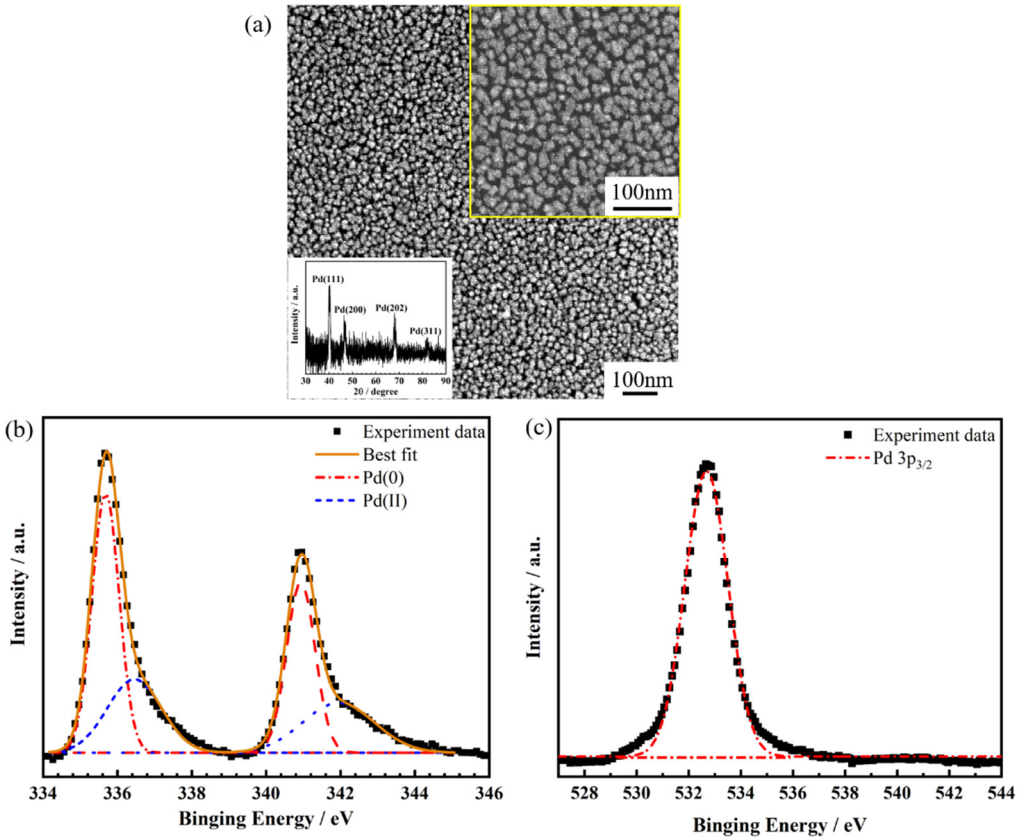

Figure 8. (**a**) SEM image of the prepared particles on Si (100) surface (The bottom-left inset is GIXRD spectrum, and top-right inset is high magnification). (**b**,**c**) experimental and fitted Pd 3d and Pd 3p spectra, respectively.

To further assess the chemical state of the palladium particles, XPS was carried out. Typical XPS spectra of the Pd $3d_{5/2}$, Pd $3d_{3/2}$, and Pd $3p_{3/2}$ levels for the particles on the Si (100) surface are shown in Figure 8b,c. The peak positions were referenced to carbon at 284.8 eV. Curve fitting analysis showed that the Pd 3d spectra resulted from two pairs of spin-orbit components. The Pd $3d_{5/2}$ peak at 335.6 eV had been attributed to metallic palladium (Pd(0)) [41] (Figure 8b). The second Pd $3d_{5/2}$ signal presenting at 336.4 eV

was due to palladium atoms with lower charge densities. The origin of such palladium species might have been due to a perturbation occurring during the dispersion process of palladium clusters [42]. For comparison, the Pd $3d_{5/2}$ signal for Pd–O was at 337.0 eV, based on Zhou et al. [43]. Also, an O 1s signal at 529.3 eV was observed [44], which did not appear in the resulting particles (Figure 8c). Hence, it was reasonable to exclude the presence of palladium oxide, which agrees with the GIXRD spectrum.

4. Conclusions

DFT simulations were used to elucidate the adsorption and reaction mechanisms for the synthesis of palladium from $Pd(hfac)_2$ and ozone on Si. The dissociative chemical absorption of $Pd(hfac)_2$ produced Pd(hfac)* and hfac*. The ozone cleaves the C–C bond located at the bridging location of Pd(hfac) to produce Pd* (activation barrier 0.46 eV). With excess ozone molecules, the Pd* formation activation barrier became 0.42 eV. The ozone molecule at the toping Pd site could reversibly bond with the Pd in Pd(hfac-O)* to produce O_3–Pd(hfac-O)* without a barrier. It could then decay to produce O–Pd(hfac-O)* and oxygen though it is kinetically less favorable (activation barrier 0.83 eV). The Pd* that was produced could further react with ozone at the Pd–Si site (activation barrier 0.64 eV). Therefore, palladium metal must be prepared by controlling the ozone condition carefully. Moreover, we prepared palladium metal successfully on the Si (100) surface without specific surface treatment (e.g., heat treatment or H_2SO_4/H_2O_2 mixture) by ALD.

Supplementary Materials: The following are available online at https://www.mdpi.com/article/10.3390/pr9122246/s1, Figure S1: Configurations of (a) 1/16 ML and (b) 3/4 ML OH/Si (100) surface., Figure S2: Optimized geometries of different adsorbed species ($Pd(hfac)_2$*(a, b), Pd(hfac)*(c) and hfac*(d)) on (a, c, d) 1/16 ML and (b) 3/4 ML OH/Si (100) surfaces.

Author Contributions: Conceptualization, C.C. and S.L.; methodology, C.C.; software, C.C.; formal analysis, C.C.; investigation, Y.Z.; data curation, J.L. and R.G.; writing—original draft preparation, C.C.; writing—review and editing, J.H., S.L. and A.I.Y.T.; visualization, A.J.O.; supervision, A.I.Y.T.; project administration, A.I.Y.T.; funding acquisition, A.I.Y.T. All authors have read and agreed to the published version of the manuscript.

Funding: This research was funded by the Agency for Science, Technology and Research (A*STAR) under award number SERC A1983c0032, AME Individual Research Grant (IRG)grant number.

Institutional Review Board Statement: Not applicable.

Informed Consent Statement: Not applicable.

Data Availability Statement: Data is contained within the article or Supplementary Materials.

Acknowledgments: The authors would like to acknowledge funding support from the Agency for Science, Technology and Research (A*STAR) under award number SERC A1983c0032, AME Individual Research Grant (IRG)grant number and the computing resources from National Supercomputing Centre Singapore.

Conflicts of Interest: The authors declare no conflict of interest.

References

1. Wang, Z.; Li, X.; Ling, H.; Tan, C.K.; Yeo, L.P.; Grimsdale, A.; Tok, A.I.Y. 3D FTO/FTO-Nanocrystal/TiO_2 Composite Inverse Opal Photoanode for Efficient Photoelectrochemical Water Splitting. *Small* **2018**, *14*, e1800395. [CrossRef] [PubMed]
2. Li, X.; Puttaswamy, M.; Wang, Z.; Tan, C.K.; Grimsdale, A.C.; Kherani, N.P.; Tok, A.I.Y. A pressure tuned stop-flow atomic layer deposition process for MoS_2 on high porous nanostructure and fabrication of TiO_2/MoS_2 core/shell inverse opal structure. *Appl. Surf. Sci.* **2017**, *422*, 536–543. [CrossRef]
3. Song, M.; Tan, H.; Li, X.; Tok, A.I.Y.; Liang, P.; Chao, D.; Fan, H.J. Atomic-Layer-Deposited Amorphous MoS_2 for Durable and Flexible Li–O_2 Batteries. *Small Methods* **2019**, *4*, 1900274. [CrossRef]
4. Dendooven, J.; Van Daele, M.; Solano, E.; Ramachandran, R.K.; Minjauw, M.M.; Resta, A.; Vlad, A.; Garreau, Y.; Coati, A.; Portale, G.; et al. Surface mobility and impact of precursor dosing during atomic layer deposition of platinum: In situmonitoring of nucleation and island growth. *Phys. Chem. Chem. Phys.* **2020**, *22*, 24917–24933. [CrossRef]

5. Van Daele, M.; Detavernier, C.; Dendooven, J. Surface species during ALD of platinum observed with in situ reflection IR spectroscopy. *Phys. Chem. Chem. Phys.* **2018**, *20*, 25343–25356. [CrossRef]
6. Feng, J.-Y.; Minjauw, M.M.; Ramachandran, R.K.; Van Daele, M.; Poelman, H.; Sajavaara, T.; Dendooven, J.; Detavernier, C. The co-reactant role during plasma enhanced atomic layer deposition of palladium. *Phys. Chem. Chem. Phys.* **2020**, *22*, 9124–9136. [CrossRef]
7. Yeo, S.; Choi, S.-H.; Park, J.-Y.; Kim, S.-H.; Cheon, T.; Lim, B.-Y.; Kim, S. Atomic layer deposition of ruthenium (Ru) thin films using ethylbenzen-cyclohexadiene Ru(0) as a seed layer for copper metallization. *Thin Solid Films* **2013**, *546*, 2–8. [CrossRef]
8. Cao, K.; Liu, X.; Zhu, Q.; Shan, B.; Chen, R. Atomically Controllable Pd@Pt Core-Shell Nanoparticles towards Preferential Oxidation of CO in Hydrogen Reactions Modulated by Platinum Shell Thickness. *ChemCatChem* **2015**, *8*, 326–330. [CrossRef]
9. Feng, Q.; Zhao, S.; Xu, Q.; Chen, W.; Tian, S.; Wang, Y.; Yan, W.; Luo, J.; Wang, D.; Li, Y. Mesoporous Nitrogen-Doped Carbon-Nanosphere-Supported Isolated Single-Atom Pd Catalyst for Highly Efficient Semihydrogenation of Acetylene. *Adv. Mater.* **2019**, *31*, 1901024. [CrossRef]
10. Li, J.; Zhong, L.; Tong, L.; Yu, Y.; Liu, Q.; Zhang, S.; Yin, C.; Qiao, L.; Li, S.; Si, R.; et al. Atomic Pd on Graphdiyne/Graphene Heterostructure as Efficient Catalyst for Aromatic Nitroreduction. *Adv. Funct. Mater.* **2019**, *29*, 1905423. [CrossRef]
11. Zhou, C.; Szpunar, J.A. Hydrogen Storage Performance in Pd/Graphene Nanocomposites. *ACS Appl. Mater. Interfaces* **2016**, *8*, 25933–25940. [CrossRef] [PubMed]
12. Zhao, Y.; Liu, F.; Tan, J.; Li, P.; Wang, Z.; Zhu, K.; Mai, X.; Liu, H.; Wang, X.; Ma, Y.; et al. Preparation and hydrogen storage of Pd/MIL-101 nanocomposites. *J. Alloys Compd.* **2018**, *772*, 186–192. [CrossRef]
13. Honarpazhouh, Y.; Astaraei, F.R.; Naderi, H.R.; Tavakoli, O. Electrochemical hydrogen storage in Pd-coated porous silicon/graphene oxide. *Int. J. Hydrog. Energy* **2016**, *41*, 12175–12182. [CrossRef]
14. Weber, M.; Kim, J.-Y.; Lee, J.-H.; Kim, J.-H.; Iatsunskyi, I.; Coy, E.; Miele, P.; Bechelany, M.; Kim, S.S. Highly efficient hydrogen sensors based on Pd nanoparticles supported on boron nitride coated ZnO nanowires. *J. Mater. Chem. A* **2019**, *7*, 8107–8116. [CrossRef]
15. Cho, S.-Y.; Ahn, H.; Park, K.; Choi, J.; Kang, H.; Jung, H.-T. Ultrasmall Grained Pd Nanopattern H_2 Sensor. *ACS Sens.* **2018**, *3*, 1876–1883. [CrossRef]
16. Kumar, M.; Bhati, V.S.; Ranwa, S.; Singh, J.; Kumar, M. Pd/ZnO nanorods based sensor for highly selective detection of extremely low concentration hydrogen. *Sci. Rep.* **2017**, *7*, 236. [CrossRef] [PubMed]
17. Yang, J.; Cao, K.; Gong, M.; Shan, B.; Chen, R. Atomically decorating of MnOx on palladium nanoparticles towards selective oxidation of benzyl alcohol with high yield. *J. Catal.* **2020**, *386*, 60–69. [CrossRef]
18. Goldstein, D.; George, S. Surface poisoning in the nucleation and growth of palladium atomic layer deposition with $Pd(hfac)_2$ and formalin. *Thin Solid Films* **2011**, *519*, 5339–5347. [CrossRef]
19. Senkevich, J.; Tang, F.; Rogers, D.; Drotar, J.; Jezewski, C.; Lanford, W.; Wang, G.-C.; Lu, T.-M. Substrate-Independent Palladium Atomic Layer Deposition. *Chem. Vap. Depos.* **2003**, *9*, 258–264. [CrossRef]
20. Elam, J.; Zinovev, A.; Han, C.; Wang, H.; Welp, U.; Hryn, J.; Pellin, M. Atomic layer deposition of palladium films on Al_2O_3 surfaces. *Thin Solid Films* **2006**, *515*, 1664–1673. [CrossRef]
21. Weber, M.J.; Mackus, A.J.M.; Verheijen, M.A.; Longo, V.; Bol, A.A.; Kessels, W.M.M. Atomic Layer Deposition of High-Purity Palladium Films from $Pd(hfac)_2$ and H_2 and O_2 Plasmas. *J. Phys. Chem. C* **2014**, *118*, 8702–8711. [CrossRef]
22. Dendooven, J.; Ramachandran, R.K.; Devloo-Casier, K.; Rampelberg, G.; Filez, M.; Poelman, H.; Marin, G.B.; Fonda, E.; Detavernier, C. Low-Temperature Atomic Layer Deposition of Platinum Using (Methylcyclopentadienyl)trimethylplatinum and Ozone. *J. Phys. Chem. C* **2013**, *117*, 20557–20561. [CrossRef]
23. Hämäläinen, J.; Munnik, F.; Ritala, M.; Leskela, M. Atomic Layer Deposition of Platinum Oxide and Metallic Platinum Thin Films from $Pt(acac)_2$ and Ozone. *Chem. Mater.* **2008**, *20*, 6840–6846. [CrossRef]
24. Park, S.-J.; Kim, W.-H.; Maeng, W.; Yang, Y.; Park, C.; Kim, H.; Lee, K.-N.; Jung, S.-W.; Seong, W. Effect oxygen exposure on the quality of atomic layer deposition of ruthenium from bis(cyclopentadienyl)ruthenium and oxygen. *Thin Solid Films* **2008**, *516*, 7345–7349. [CrossRef]
25. Zou, Y.; Cheng, C.; Guo, Y.; Ong, A.J.; Goei, R.; Li, S.; Tok, A.I.Y. Atomic layer deposition of rhodium and palladium thin film using low-concentration ozone. *RSC Adv.* **2021**, *11*, 22773–22779. [CrossRef]
26. Kresse, G.; Hafner, J. Ab initiomolecular dynamics for liquid metals. *Phys. Rev. B* **1993**, *47*, 558–561. [CrossRef]
27. Kresse, G.; Furthmüller, J. Efficiency of ab-initio total energy calculations for metals and semiconductors using a plane-wave basis set. *Comput. Mater. Sci.* **1996**, *6*, 15–50. [CrossRef]
28. Blöchl, P.E. Projector augmented-wave method. *Phys. Rev. B* **1994**, *50*, 17953–17979. [CrossRef]
29. Kresse, G.; Joubert, D. From ultrasoft pseudopotentials to the projector augmented-wave method. *Phys. Rev. B* **1999**, *59*, 1758. [CrossRef]
30. Perdew, J.P.; Burke, K.; Ernzerhof, M. Generalized gradient approximation made simple. *Phys. Rev. Lett.* **1996**, *77*, 3865. [CrossRef]
31. Chadi, D.J. Special points for Brillouin-zone integrations. *Phys. Rev. B* **1976**, *13*, 5188–5192. [CrossRef]
32. Henkelman, G.; Uberuaga, B.P.; Jónsson, H. A climbing image nudged elastic band method for finding saddle points and minimum energy paths. *J. Chem. Phys.* **2000**, *113*, 9901–9904. [CrossRef]
33. Henkelman, G.; Jónsson, H. Improved tangent estimate in the nudged elastic band method for finding minimum energy paths and saddle points. *J. Chem. Phys.* **2000**, *113*, 9978–9985. [CrossRef]

34. Lei, Y.; Liu, B.; Lu, J.; Lin, X.; Gao, L.; Guisinger, N.P.; Greeley, J.P.; Elam, J.W. Synthesis of palladium nanoparticles on TiO_2(110) using a beta-diketonate precursor. *Phys. Chem. Chem. Phys.* **2015**, *17*, 6470–6477. [CrossRef]
35. Palummo, M.; Onida, G.; Del Sole, R.; Mendoza, B.S. Ab initiooptical properties of Si(100). *Phys. Rev. B* **1999**, *60*, 2522. [CrossRef]
36. Lu, X.; Zhang, Q.; Lin, M.C. Adsorption of methanol, formaldehyde and formic acid on the Si(100)-2×1 surface: A computational study. *Phys. Chem. Chem. Phys.* **2001**, *3*, 2156–2161. [CrossRef]
37. Siedle, A.R.; Newmark, R.A.; Pignolet, L.H. Structure of palladium bis (hexafluoroacetylacetonate) and the systematics of its acid-base chemistry. *Inorg. Chem.* **1983**, *22*, 2281–2286. [CrossRef]
38. Basova, T.; Kiselev, V.; Filatov, E.S.; Sheludyakova, L.A.; Igumenov, I.K. Experimental and theoretical study of vibrational spectra of palladium(II) β-diketonates. *Vib. Spectrosc.* **2012**, *61*, 219–225. [CrossRef]
39. Goldstein, D.N.; McCormick, J.A.; George, S. Al_2O_3 Atomic Layer Deposition with Trimethylaluminum and Ozone Studied by in Situ Transmission FTIR Spectroscopy and Quadrupole Mass Spectrometry. *J. Phys. Chem. C* **2008**, *112*, 19530–19539. [CrossRef]
40. Elliott, S.D.; Scarel, G.; Wiemer, A.C.; Fanciulli, M.; Pavia, G. Ozone-Based Atomic Layer Deposition of Alumina from TMA: Growth, Morphology, and Reaction Mechanism. *Chem. Mater.* **2006**, *18*, 3764–3773. [CrossRef]
41. Wagner, C.D.; Naumkin, A.V.; Kraut-Vass, A.; Allison, J.W.; Powell, C.J.; Rumble, J.R., Jr. *NIST Standard Reference Database*; Version 3.4 (Web Version); US Department of Commerce: Washington, DC, USA, 2003. Available online: https://www.nist.gov/srd (accessed on 15 February 2021).
42. Evangelisti, C.; Panziera, N.; Pertici, P.; Vitulli, G.; Salvadori, P.; Battocchio, C.; Polzonetti, G. Palladium nanoparticles supported on polyvinylpyridine: Catalytic activity in Heck-type reactions and XPS structural studies. *J. Catal.* **2009**, *262*, 287–293. [CrossRef]
43. Zhou, X.; Goh, S.; Lee, S.; Tan, K. X-ray photoelectron spectroscopic studies of ionic interactions in poly(styrenesulfonic acid)/poly(vinylpyridine) complexes. *Appl. Surf. Sci.* **1998**, *126*, 141–147. [CrossRef]
44. Kim, K.S.; Gossmann, A.F.; Winograd, N. X-ray photoelectron spectro-scopic studies of palladium oxides and the palladium-oxygen electrode. *Anal. Chem.* **1974**, *46*, 197–200. [CrossRef]